



## Post-irradiation intratumoral heterogeneity modulates response to immune checkpoint inhibition therapy in a murine melanoma model



Jie Wang<sup>a,b,d,#</sup>, Shivani Sud<sup>a,#</sup>, Yanli Qu<sup>e</sup>, Liantao Li<sup>a,f</sup>, Jiajie Zhang<sup>a,g</sup>, David Marron<sup>c</sup>, Nicole Michelle Knappe<sup>a</sup>, Isaiah James Kim<sup>a</sup>, Kyle Thomas Wagner<sup>a</sup>, Tian Zhang<sup>h,i</sup>, Yuxia Zhao<sup>b</sup>, Geyan Guo<sup>a,b</sup>, Andrew Z. Wang<sup>a,j,\*</sup>

<sup>a</sup> Department of Radiation Oncology University of North Carolina-Chapel Hill, Chapel Hill, NC

<sup>b</sup> Department of Radiation Oncology, The Fourth Affiliated Hospital of China Medical University, Shenyang, Liaoning China, 110032

<sup>c</sup> Lineberger Comprehensive Cancer Center, University of North Carolina at Chapel Hill, Chapel Hill, NC

<sup>d</sup> Department of Radiation Oncology, Dalian Municipal Central Hospital, Dalian, Liaoning China, 116033

<sup>e</sup> Department of Thoracic Radiation Oncology, Cancer Hospital of China Medical University, Liaoning Cancer Hospital & Institute, Shenyang, China, 110042

<sup>f</sup> Center of Clinical Oncology, Affiliated Hospital of Xuzhou Medical University, Xuzhou, China

<sup>g</sup> Department of Pancreatic Surgery, Huashan Hospital, Fudan University, Shanghai, China, 200040

<sup>h</sup> Division of Medical Oncology, Department of Medicine, Duke Cancer Institute, Duke University, Durham, NC

<sup>i</sup> Department of Medicine, Harold C. Simmons Comprehensive Cancer Center, University of Texas Southwestern Medical Center, Dallas, TX

<sup>j</sup> Department of Radiation Oncology, University of Texas Southwestern Medical Center, Dallas, TX

### ARTICLE INFO

Editor: Prof Alnawaz Rehemtulla

#### Keywords:

radiation therapy  
immunotherapy  
checkpoint inhibition  
tumor mutational burden  
intra-tumor heterogeneity  
neoantigen  
*in situ* vaccine

### ABSTRACT

**Purpose:** The underlying mechanism for radiation as a potentiator of immune checkpoint inhibition (ICI) is unclear. We developed a novel murine model to investigate the effects of post-irradiation intratumoral heterogeneity (ITH) on response to ICI.

**Experimental design:** Parental mouse melanoma B16F10 cells were irradiated *in vitro* (5Gy x 3 fractions), then an *a priori* determined number of resulting colonies were implanted in C57BL/6J immunocompetent mice creating syngeneic models of unirradiated (parental) and irradiated tumors with low (irradiated-L) and high (irradiated-H) ITH. Mice were treated with placebo,  $\alpha$ -PD-L1,  $\alpha$ -CTLA-4 or dual ICI. Murine tumors underwent whole exome sequencing (WES). Clinically correlated paired pre- and post-irradiation patient rectal adenocarcinoma samples underwent WES.

**Results:** Irradiated-L tumors showed increased tumor mutational burden (TMB) and a sustained decrease in ITH. Irradiated-L tumors were predicted to express five neoantigens with high variant allele frequency/clonal distribution. Mice with irradiated-L and irradiated-H versus parental B16F10 tumors demonstrated longer overall survival with dual ICI. Only mice with irradiated-L tumors experienced an overall survival benefit with single agent ICI. Clinically correlated rectal adenocarcinoma samples showed similarly increased TMB and decreased ITH following irradiation.

**Conclusions:** Post-irradiation ITH modulates ICI response in a murine melanoma model. Irradiation may offer a mechanism to widen the therapeutic window of ICI.

**Abbreviations:** ICI, Immune checkpoint inhibition; TMB, Tumor mutational burden; ITH, Intratumoral heterogeneity; VAF, Variant Allele Frequency; PD-L1, Programmed death ligand 1; PD-1, Programmed death 1; CTLA4, Cytotoxic T-Lymphocyte Associated Protein 4; PFS, Progression free survival; NSCLC, Non-small cell lung cancer; WES, Whole exome sequencing; SNV, Single nucleotide variant.

\* Corresponding author.

**E-mail addresses:** [wangjiezyy@icloud.com](mailto:wangjiezyy@icloud.com) (J. Wang), [shivani.sud@unchealth.unc.edu](mailto:shivani.sud@unchealth.unc.edu) (S. Sud), [qyanli@cancerhosp-ln-cmu.com](mailto:qyanli@cancerhosp-ln-cmu.com) (Y. Qu), [liliantao@xzhmu.edu.cn](mailto:liliantao@xzhmu.edu.cn) (L. Li), [16111220055@fudan.edu.cn](mailto:16111220055@fudan.edu.cn) (J. Zhang), [dmarron@cs.unc.edu](mailto:dmarron@cs.unc.edu) (D. Marron), [Nicole\\_Knappe@med.unc.edu](mailto:Nicole_Knappe@med.unc.edu) (N.M. Knappe), [isaiah\\_kim@med.unc.edu](mailto:isaiah_kim@med.unc.edu) (I.J. Kim), [kyle.t.wagner@outlook.com](mailto:kyle.t.wagner@outlook.com) (K.T. Wagner), [tian.zhang@utsouthwestern.edu](mailto:tian.zhang@utsouthwestern.edu) (T. Zhang), [zhaoyx2019@hotmail.com](mailto:zhaoyx2019@hotmail.com) (Y. Zhao), [gyguo@cmu.edu.cn](mailto:gyguo@cmu.edu.cn) (G. Guo), [andrew.wang2@utsouthwestern.edu](mailto:andrew.wang2@utsouthwestern.edu) (A.Z. Wang).

# These authors contributed equally to this work.

<https://doi.org/10.1016/j.neo.2022.100864>

Received 12 April 2022; Received in revised form 6 December 2022; Accepted 12 December 2022

1476-5586/© 2022 The Authors. Published by Elsevier Inc. This is an open access article under the CC BY-NC-ND license (<http://creativecommons.org/licenses/by-nc-nd/4.0/>)

## Background

Immunotherapy yields a durable response and survival benefit in many previously treatment refractory malignant tumors, yet response rates remain low (~15%-25% across tumor types) [1]. Thus, strategies to overcome immunotherapy resistance are needed. Immune checkpoint inhibitors (ICI) in clinical use include monoclonal antibodies that block tumor programmed death ligand 1 (PD-L1) binding to T cell programmed death 1 (PD-1) and antigen-presenting cell B7 ligand binding to T cell receptor CTLA-4. A growing body of evidence provides support for combining radiation with ICI [2,3]. However, clinical trials results show mixed results providing an impetus to characterize and exploit presently unknown determinants of efficacy of ICI as part of radiation-based treatment paradigms.

Proposed mechanisms of radiation-mediated potentiation of ICI include immunomodulation of the tumor microenvironment and *in situ* vaccination – wherein neoantigens arising from patient-specific somatic mutations within the tumor stimulate an effective antitumor T cell response [4,5]. Tumor mutational burden (TMB) is independently associated with improved response to immunotherapy, however, non-irradiated tumors with high TMB have highly variable responses to checkpoint inhibitors; the ability of radiation to induce TMB sufficient to drive immunotherapy response is debated [6–8]. High levels of predicted epitope producing immunogenic mutations correlate with anti-tumor cytotoxic T cell responses across various tumor types [9,10]. For example, in chemo-refractory metastatic NSCLC, radiation with anti-CTLA-4 therapy induced a systemic T cell response via a proposed mechanism of radiation-induced exposure of immunogenic mutations to the immune system [11]. Mutational intratumoral heterogeneity (ITH) may facilitate tumor adaptation and poor treatment response via corresponding heterogeneity in protein function [12] and neoantigen expression [13]. High burden of clonal, but not subclonal, tumor neoantigens correlate with T cell response and clinical benefit of checkpoint inhibitors providing support for a dominant role of clonal neoantigens [13]. In melanoma, murine models and clinical data show tumors with low ITH, independent of TMB, are more responsive to checkpoint inhibitors [14].

We have developed a syngeneic model of unirradiated and irradiated melanoma tumors with defined states of low- and high- ITH. In the present study we characterize the role of ITH post-irradiation on response to ICI. Our preclinical model is supported by corresponding findings in clinically correlated samples.

## Methods

### Tumor cell line and culture conditions

Mouse skin melanoma cell line B16F10 (ATCC, Manassas, VA) was maintained in Dulbecco's Modified Eagle's Medium supplemented with 10% fetal bovine serum, 2 mM L-glutamine, 100 U/mL penicillin and 100 µg/mL streptomycin (Mediatech). Cells were incubated at 37°C in a humidified chamber containing 5% CO<sub>2</sub>.

### Cell line irradiation and characterization

To develop models of unirradiated and irradiated tumors with low- and high- ITH (irradiated-L and irradiated-H, respectively), parental B16F10 cells were irradiated *in vitro* to control ITH at the time of implantation and facilitate accurate TMB characterization of resultant tumors [Fig. 1A]. Parental B16F10 cells were initially maintained in a 75cm<sup>2</sup> flask prior to irradiation with an X-RAD 320 irradiator (Precision X-Ray, Inc., North Branford, CT) to a total dose of 15 Gy given in 3 fractions. To generate the irradiated-L model, following the first fraction of irradiation (5Gy) and recovery to 40-60% confluence, per clonogenic assay protocol, cells were seeded into six-well plates with 20 cells per well. Following recovery to 40-60% confluence the cells were re-irradiated (5Gy). The latter step was repeated once again to reach a total dose of

15Gy. To generate the irradiated-H model, following the first fraction of irradiation (5Gy) and recovery to 40-60% confluence, 1000 irradiated cells were seeded in a 75cm<sup>2</sup> flask. Following recovery to 40-60% confluence the cells were re-irradiated (5Gy). The latter step was repeated once again to reach a total dose of 15Gy. The average final number of colonies present in each well (irradiated-L) or flask (irradiated-H) that were harnessed for injection at the end of the full radiation course was calculated based on the average surviving fraction wherein the number of colonies present following each fraction is equal to the surviving fraction multiplied by the number of cells seeded multiplied by the plating efficiency.

### Murine tumor models and *in vivo* experiments

Female, 6-8 weeks old C57BL/6J mice (The Jackson Laboratory, Bar Harbor, Maine) were cared for per protocols approved by the University of North Carolina Animal Care and Use Committee. Three mouse models, unirradiated parental B16F10, irradiated-L, and irradiated-H were established with right flank injection of  $5.0 \times 10^4$  cells of the parental B16F10 cell line or an *a priori* determined number of colonies from irradiated cell lines suspended in FBS-free DMEM medium and Matrigel (BD Biosciences) in a 1:1 ratio on day 0. For each mouse model we established four ICI treatment groups, control (placebo),  $\alpha$ -PD-L1,  $\alpha$ -CTLA4, and dual ICI. Mouse anti-PD-L1 ( $\alpha$ -PD-L1) 10ug/g (clone 10F.9G2), mouse anti-CTLA4 ( $\alpha$ -CTLA4) 5ug/g (clone 9D9) antibodies (Bioxcell) were delivered via intraperitoneal injection on days 3, 6 and 9 [Fig. 1B].

Three times weekly, mice were monitored for toxicity and tumors were measured with digital calipers via two independent measurements including at least one measurement by a researcher blinded to treatment group. Mice were euthanized with CO<sub>2</sub> asphyxiation once tumors reached 2000mm<sup>3</sup>, exceeded 20mm in any dimension, or upon presence of moribund behavior. Tumors were dissected en bloc and frozen in liquid nitrogen.

### Murine model whole-exome sequencing and somatic mutation calling

Genomic DNA isolation from fresh frozen tumors was performed per manufacturer's protocol with the DNeasy Blood & Tissue Kit (Qiagen). Whole exome libraries were constructed with genomic DNA and the SureSelectXT Mouse All Exon kit (Agilent Technologies, CA, USA) designed to enrich the complete mouse exome including 221,784 exons from 24,306 genes, covering 49.6 Mb per manufacturer's protocol. Genomic DNA was sheared to 200bp using a LE220 Focused-ultrasonicator (Covaris) prior to library construction. Genomic DNA library quality and quantity were assessed using a 2200 TapeStation and High Sensitivity D1000 ScreenTape (Agilent), respectively. Exome libraries were sequenced using the Illumina HiSeq 2500 platform. Paired-end reads (2 × 150 bp) were generated using a mean depth of 100X. Sequencing reads were mapped to the mouse genome (UCSC mm10) using the Burrows-Wheeler Alignment Maximal Exact Matches algorithm (BWA-MEM) (v2.18.29) [15] per developer default parameters. Duplicates were removed with Picard (v2.18.29). Somatic variations were called with GATK4 Mutect2 [16], filtered against C57BL/6c as a panel of normal and variants were annotated using ANNOVAR [17] and Variant Effect Predictor (VEP v84) [18]. Changes in clonal architecture between paired parental B16F10 and irradiated-L tumors were evaluated using SNVs detected using whole exome sequencing (WES) data for Irradiated-L versus Parental B16F10 tumors following harvest and the fishplot package for R analysis pipeline [19].

### Murine model prediction of candidate neoantigens

Genes with <10 transcripts on WES were filtered and neoantigen predictions were performed using pVAC-Seq (version 1.5.1) with a MHC binding affinity IC<sub>50</sub> ≤ 500 nmol/L threshold following published guidelines [20]. Expression of predicted neoantigens was validated with RNA

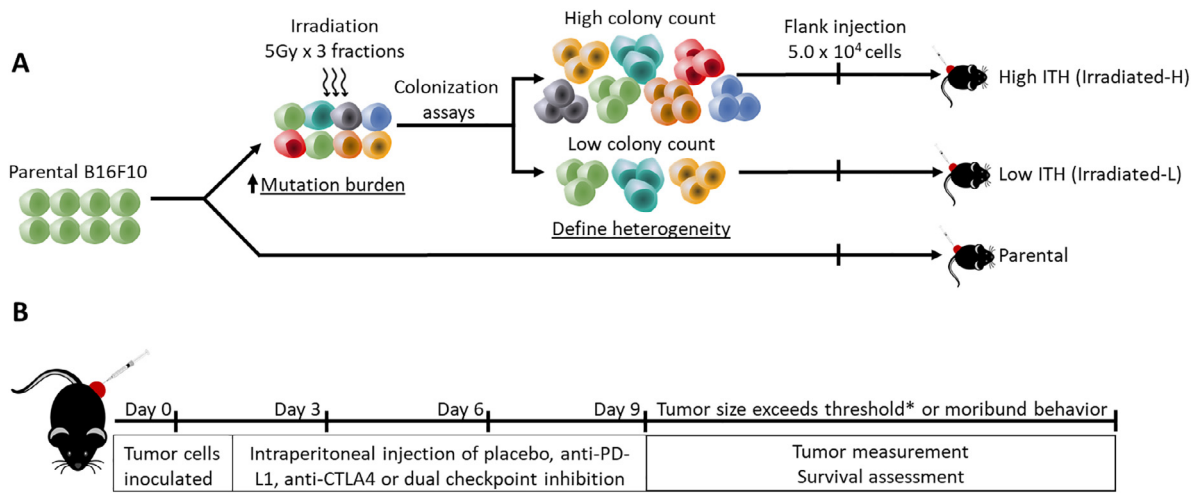


**Fig. 1.** Development of a murine melanoma model with defined states of tumor mutational burden and intratumoral heterogeneity (ITH) to elucidate the mechanisms through which irradiation potentiates checkpoint inhibition. **A.** Mouse skin melanoma B16F10 cells were irradiated *in vitro* with 5Gy x 3 fractions and passed between fractions. Colonization assays were performed to facilitate clonal expansion of cells surviving irradiation. Three mouse models were established with right flank injection of  $5.0 \times 10^4$  cells of parental cell line B16F10 (parental B16F10) or an *a priori* determined number of colonies from irradiated cell lines to generate tumors with low (irradiated-L) and high ITH (irradiated-H). **B.** For each mouse model we established four ICI treatment groups, control (placebo),  $\alpha$ -PD-L1,  $\alpha$ -CTLA4, and dual ICI.

sequencing. Tumor messenger RNA was isolated with the RNeasy Mini Kit (Qiagen) and heat fragmented for preparation of poly(A)-selected RNA libraries using the TruSeq RNA library (Illumina) per manufacturer’s protocol. Pooled, normalized c-DNA libraries were run on a HiSeq 2500 sequencer (Illumina) with paired-end reads ( $2 \times 150$  bp). Sequencing reads were aligned to the mouse mm10 reference genome using STAR (version 2.6.0c) [21] and transcript read counts were determined using RSEM (version 1.2.28) [22].

*Patient and sample characteristics*

To validate murine model results demonstrating the effect of radiation on TMB and ITH with clinical correlates, 5 paired (pre- and post-radiation) tissue specimens (three intra-tumor locations to ensure adequate spatial sampling) and peripheral blood mononuclear cells (PBMCs) were obtained from human subjects with pathologically confirmed rectal adenocarcinoma, ct3N0-2. Per standard of care at the Liaoning Cancer Hospital & Institute in China, patients received neoadjuvant chemoradiation (2.14 Gy x 24 fractions = 51.36 Gy) with concurrent oral capecitabine then resection and subsequent adjuvant therapy per provider’s discretion. Pre-radiation tissue specimens were Formalin-Fixed Paraffin-Embedded (FFPE) at time of biopsy. Post-radiation resected tissue was frozen in liquid nitrogen. The Institutional Review Board approved this study.

*Whole Exome Sequencing and somatic mutation calling*

DNA was isolated using DNA FFPE, DNAeasy and DNA blood mini kits (Qiagen) for FFPE, fresh frozen tissue and PBMCs, respectively per manufacturer’s protocols. Genomic DNA was fragmented to 200bp using the ME220 Focused-ultrasonicator (Covaris). WES libraries were constructed with the SureSelectXT Human All Exon Kit V6 (Agilent Technologies, CA) and sequenced on the HiSeq 2500 (Illumina) with paired-end reads ( $2 \times 150$ bp), mean depth 200X. Genomic DNA library quantity and quality were assessed using a Qubit fluorometer (Thermo Fisher) and 2100 Bioanalyzer System (Agilent), respectively. High quality paired end reads were aligned to the NCBI human reference genome (GRCh38/hg38) using BWA-MEM, v0.7.15-r1140. Duplicates were removed with Picard v.2.2.1 [23] and mutations were called using GATK HaplotypeCaller [24]. Somatic variants were detected using GATK4 Mutect2 (v.4.0) [25], genetic variants were annotated with ANNOVAR

[26], the effects of gene variants were predicted using Ensembl Variant Effect Predictor [18] and chromosome copy number alterations for murine and human samples were characterized using Control-FREEC [27].

*Statistical analysis*

Tumor growth curves were analyzed using two-way ANOVA for variables of time and tumor volume with Bonferroni’s multiple-comparison correction. Survival curves were generated per the Kaplan–Meier method and compared with the log-rank (Mantel-Cox) test. Statistical analyses were performed in GraphPad Prism 8.0. P-values  $\leq 0.05$  were considered significant and are indicated on figures as \* $p \leq 0.05$ , \*\* $p < 0.01$ , \*\*\* $p < 0.005$ .

*Study Approval*

Murine studies were performed per protocols approved by the University of North Carolina Animal Care and Use Committee. The Institutional Review Board of the Liaoning Cancer Hospital & Institute in China approved the human tissue studies.

**Results**

We established a syngeneic murine melanoma model with defined states of heterogeneity to enable characterization of functional irradiation-induced increases in TMB and the impact of ITH on tumor growth and survival in response to  $\alpha$ -CTLA-4 and  $\alpha$ -PD-L1 therapy (Fig. 1). Following irradiation of the parental B16F10 cell line (5 Gy x 3 fractions), we implanted a uniform number of tumor cells pooled from a known number of colonies, 5.4 and 256, respectively, to establish flank tumors in immunocompetent mice with defined states of low (irradiated-L) and high (irradiated-H) ITH. WES of parental and irradiated-L tumors showed irradiation increased TMB by 618 exon mutations including 587 single nucleotide variants (SNV), 31 insertion/deletions (indel), Fig. 2A, and induced chromosome copy number alterations (Supplementary Figure 1A). The most common SNV were T>G (32%) and C>T (21%), Fig. 2B. Irradiation led to predicted expression of five neoantigens in the following genes: Olf344, Serpina3a, Pcdhb4, Olfr1318 and Herpud2 (Table 1). Three of the five mutant epitopes had higher predicted binding affinity than the corresponding wild type epitope. Each

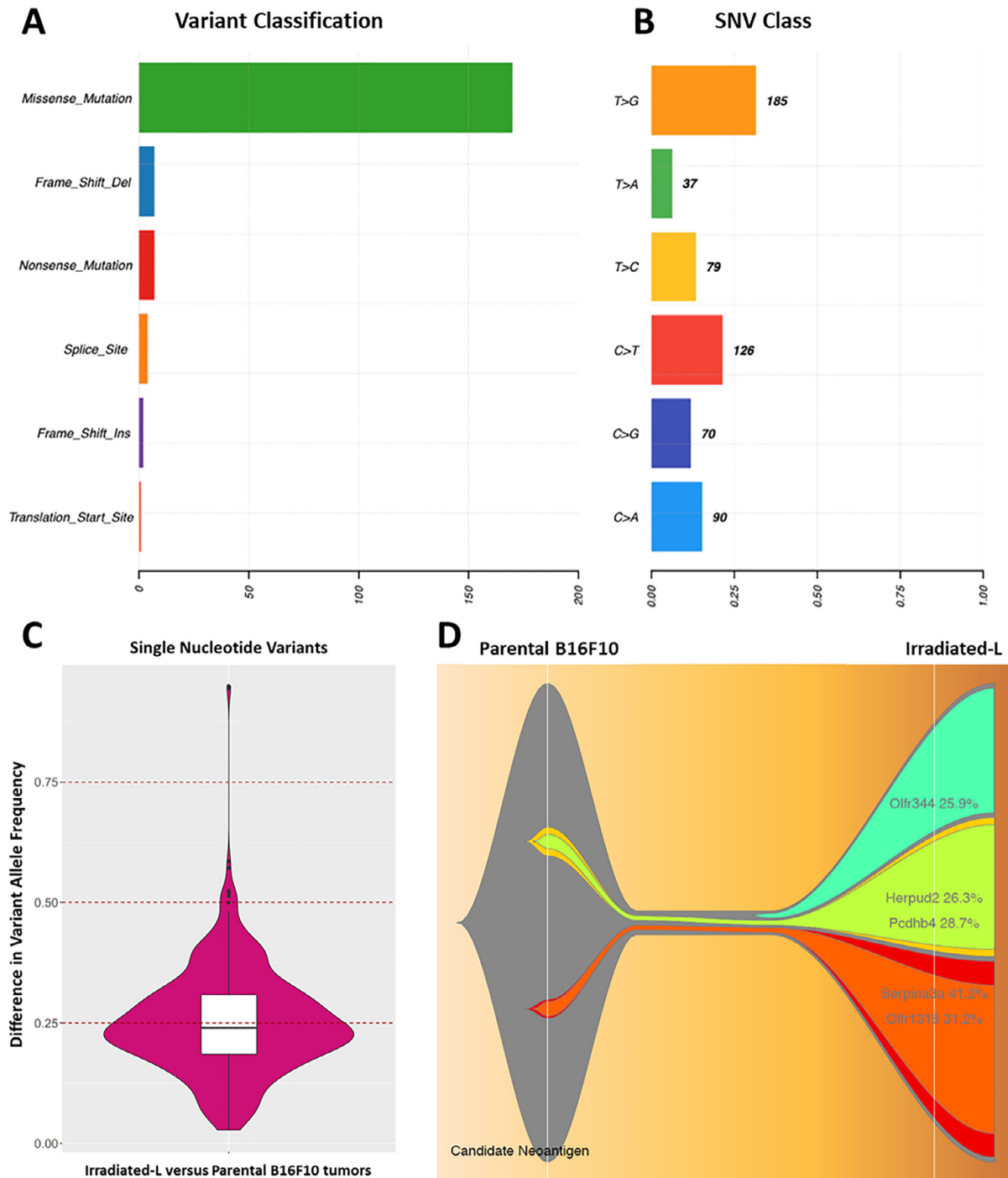


**Fig. 2.** Tumor mutation burden and variant allele frequency shifts between parental B16F10 and irradiated-L tumors on whole exome sequencing. **A.** Histogram with frequency of identified mutational classes **B.** Histogram with frequency of single nucleotide variants **C.** Violin plot of variant allele frequencies in irradiated-L versus parental B16F10 tumors. Exome sequencing detected substantial increases in variant allele frequency (median 0.24, interquartile range 0.19-0.31, minimum 0.028, maximum 0.49). **D.** Fish plot showing a bottleneck followed by subsequent clonal evolution and diminished intratumoral genetic heterogeneity between parental B16F10 and irradiated-L tumors. Informative SNVs and corresponding displayed VAF detected during whole-exome sequencing were used for subclonal detection.

neoantigen was predicted to have a public/clonal distribution (variant allele frequency, VAF, > 0.25). Expression of predicted neoantigens was confirmed on messenger RNA sequencing. On exome-wide comparison, somatic mutation VAF increased between irradiated-L versus parental tumors reflecting decreased ITH (median increase 0.24, interquartile range 0.19-0.31, minimum 0.028, maximum 0.49), **Fig. 2C**. To evaluate whether detected neoantigens arose *de novo* or reflected clonal expansion, we compared SNV profiles on WES and predicted neoantigen VAF

between irradiated-L versus parental tumors after harvest. Following a bottleneck due to inoculation of a limited number of colonies, irradiated-L tumors showed clonal expansion of both irradiation-induced *de novo* neoantigens and a subset of neoantigens harbored in parental tumors with high VAF reflecting a sustained decrease in neoantigen heterogeneity (**Fig. 2D**).

To discriminate between the functional effects of irradiation-induced TMB and ITH on tumor growth *in vivo*, we quantified tumor growth

**Table 1**  
Murine neoantigen prediction in irradiated-L tumors.

| Gene Name                              | Olfr344   | Serpina3a | Pcdhb4    | Olfr1318  | Herpud2   |
|--|-----------|-----------|-----------|-----------|-----------|
| Mutation                               | L/P       | D/Y       | F/L       | K/T       | F/V       |
| Protein Position                       | 63        | 198       | 708       | 128       | 390       |
| Mutation Position                      | 6         | 3         | 4         | 2         | 9         |
| Mutant Epitope Sequence                | PMYFFPSHL | VSYLHRNTS | VLLLMGARL | CTPLHYLTI | SAWSFITTV |
| Best mutant epitope score <sup>*</sup> | 46.07     | 166.96    | 250.1     | 114.95    | 33.4      |
| Wild type epitope score <sup>†</sup>   | 23.18     | 8571.13   | 197.8     | 1183.39   | 60.5      |
| Fold Change <sup>‡</sup>               | 0.503     | 51.336    | 0.791     | 10.295    | 1.811     |
| Tumor DNA Depth                        | 572       | 320       | 366       | 295       | 171       |
| Tumor DNA VAF                          | 0.259     | 0.412     | 0.287     | 0.312     | 0.263     |

<sup>\*</sup> Lowest half maximal inhibitory concentration (IC50) binding affinity of all prediction algorithms used.

<sup>†</sup> IC50 binding affinity of the wild type epitope.

<sup>‡</sup> IC50 binding affinity of the wild type epitope divided by the best mutant epitope score. VAF: Variant allele frequency.

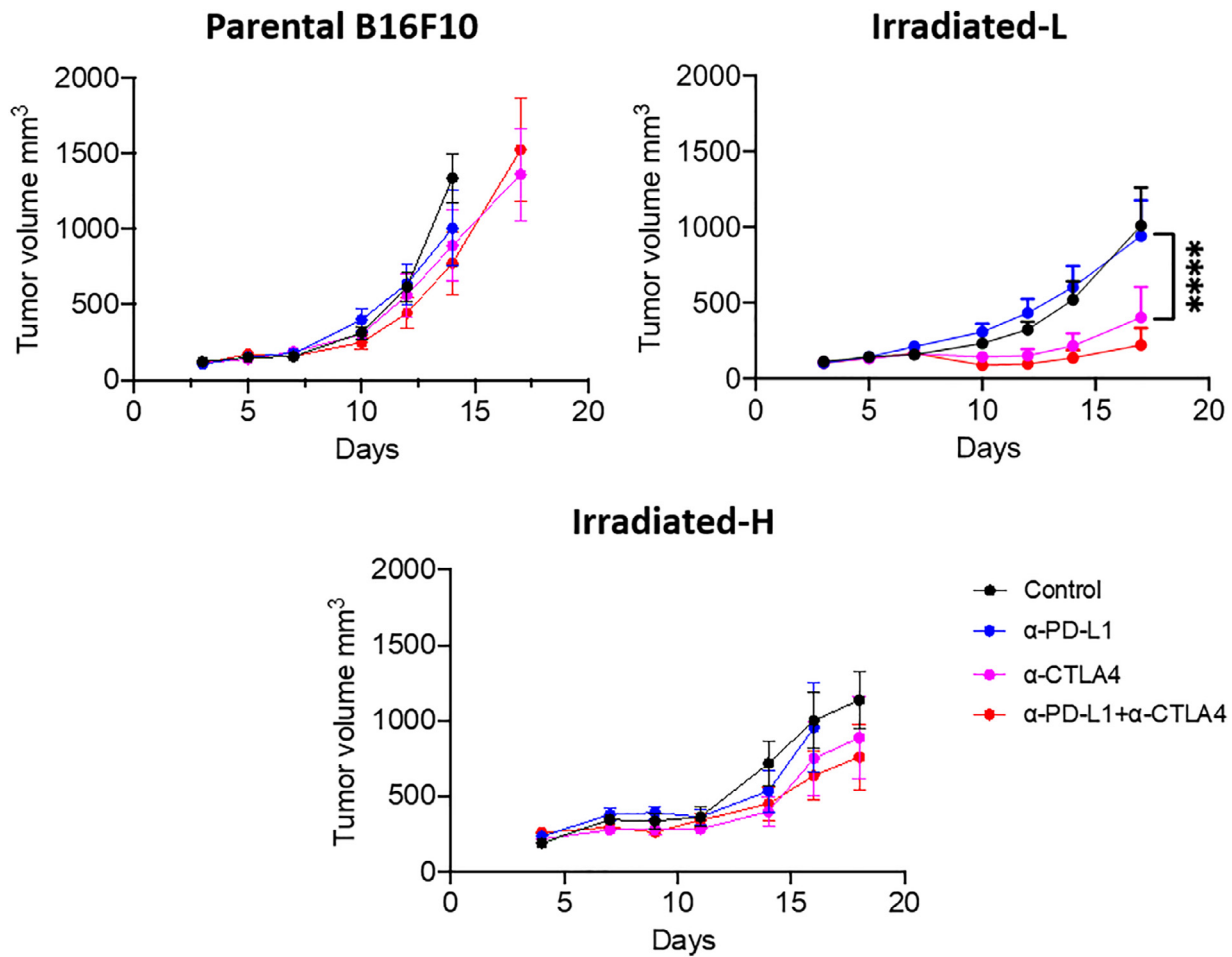


**Fig. 3.** Tumor growth curves for parental B16F10 tumors, irradiated-L and irradiated-H according to treatment groups: control,  $\alpha$ -PD-L1,  $\alpha$ -CTLA-4 and combination  $\alpha$ -PD-L1/ $\alpha$ -CTLA-4. Number of mice per treatment group, n = 10 for parental B16F10 and irradiated L, n = 8 for irradiated-H. Tumors were measured 3 times per week. Mice were euthanized once tumors reached 2000mm<sup>3</sup>, exceeded 20mm in any dimension, or upon presence of moribund behavior. When treated with dual checkpoint inhibition, tumors derived from irradiated-L grew at a significantly lower rate versus control (p<0.0001, Bonferroni's multiple comparisons test). Error bars denote the standard error of the mean (SEM).

rate and survival in parental, irradiated-L and irradiated-H control cohorts receiving placebo and cohorts receiving treatment with  $\alpha$ -CTLA-4,  $\alpha$ -PD-L1, or dual  $\alpha$ -PD-L1/ $\alpha$ -CTLA-4 checkpoint blockade (Fig. 3). Irradiated-L and irradiated-H tumors grew slower than parental tumors (Fig. 3, Supplementary Figure 2). Average tumor volumes on day 14 were as follows parental 1196 mm<sup>3</sup>, irradiated-L 519 mm<sup>3</sup> (versus parental, p = 0.001) and irradiated-H 716 mm<sup>3</sup> (versus parental

p = 0.0291) corresponding to a modest improvement in median overall survival for mice with irradiated tumors treated with placebo (irradiated-L 22.5d, irradiated-H 22d, parental 18d, p = 0.0015).

Mice with unirradiated parental tumors did not benefit from treatment with ICI (median survival, control: 18d,  $\alpha$ -PD-L1: 20d,  $\alpha$ -CTLA4: 21.5d, dual ICI: 21, p = 0.066), Fig. 4. When treated with dual ICI, irradiated-L tumors grew significantly slower than control tumors

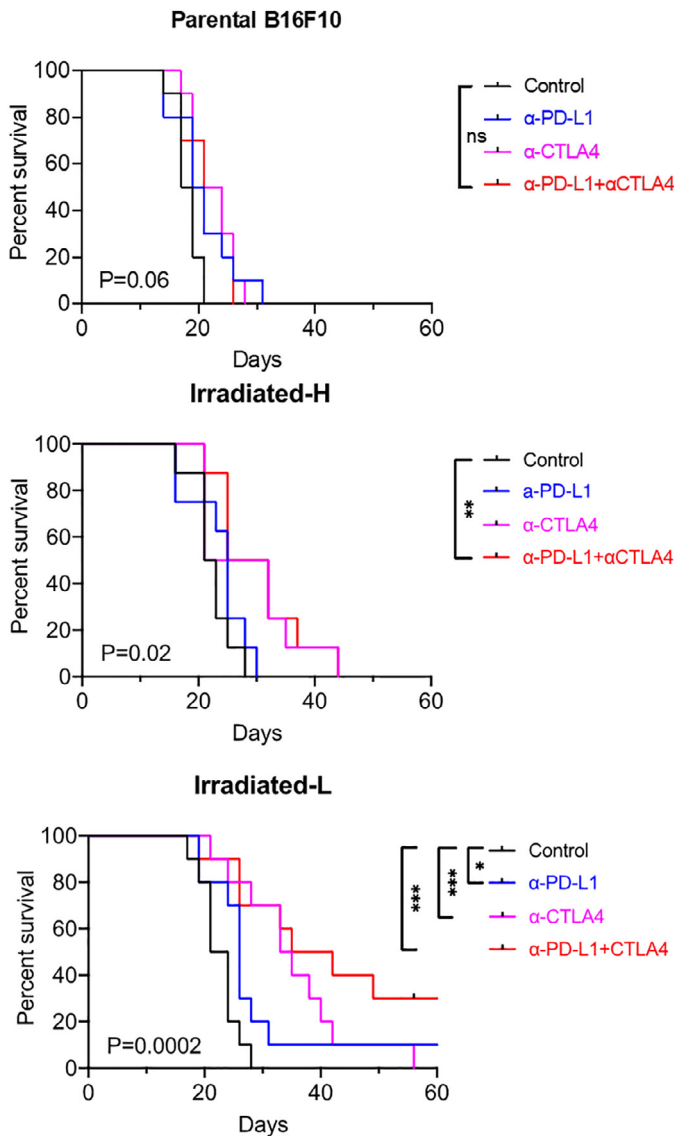


**Fig. 4.** Survival curves for parental B16F10 tumors, irradiated-L and irradiated-H by treatment groups: control,  $\alpha$ -PD-L1,  $\alpha$ -CTLA-4 and combination  $\alpha$ -PD-L1/ $\alpha$ -CTLA-4. Number of mice per treatment group, n = 10 for parental B16F10 and irradiated-L, n = 8 for irradiated-H. Mice with irradiated-L tumors had a survival benefit (versus control median 22.5d) with single agent  $\alpha$ -PD-L1 (median 26d, p = 0.046),  $\alpha$ -CTLA-4 (median 34d, p = 0.0004) and dual checkpoint inhibitor therapy (median 38.5d, p = 0.0005). Mice with irradiated-H tumors experienced increased survival (versus control 22d) with combination  $\alpha$ -PD-L1/ $\alpha$ -CTLA-4 (median 28.5d, p = 0.0075).

(Fig. 3) and overall survival was highest in the irradiated-L model (irradiated-L 38.5d, irradiated-H 28.5d, parental 21d, p = 0.0004), Fig. 4. Only the irradiated-L model showed a survival benefit with single agent  $\alpha$ -PD-L1 (median survival 26d, p = 0.046),  $\alpha$ -CTLA-4 (median survival 34d, p = 0.0004) and dual ICI (median survival 38.5d, p = 0.0005), Fig. 4. The irradiated-H model showed increased overall survival with combination  $\alpha$ -PD-L1/ $\alpha$ -CTLA-4 (irradiated-H, median survival 28.5d, p = 0.0075). On pairwise comparison, the irradiated-L model showed a greater improvement in overall survival with dual ICI than the irradiated-H model (median survival 38.5d versus 28.5d, p = 0.045).

The treatment paradigm for rectal adenocarcinoma includes neoadjuvant irradiation, resection and consideration of adjuvant therapy offering an opportunity to investigate irradiation-induced changes in TMB

and ITH through comparison of pre- and post-irradiation tissue from biopsy and resection, respectively. Five sets of paired tissue were obtained from patients with pathologically confirmed rectal cancer prior to and following neoadjuvant radiation with concurrent oral capecitabine, a radiosensitizer. Matched normal PBMCs from each patient served as a paired control during sequencing analysis. WES of pre- and post-neoadjuvant therapy tumors showed neoadjuvant therapy caused chromosome copy number alterations (Supplementary Figure 1B), and increased TMB by a median of 209 exon mutations (range 168-246) including SNV (median 173, range 154-221) and indel (median 14, range 8-73) leading primarily to missense mutations (Fig. 5A). The most common mutation signatures were T>C (31%) and C>T (38%) (Fig. 5B). Mutations were most common in *MUC12*, *PCDHB10*, *ORIS2*, *ORIS1*, *LARP4*, *PRAMEF10*, *NBPF9*, *ATP8*, *ANKRD36C*, and *AGAP4* (Fig. 5C). On exome-wide comparison for each of the five paired samples, somatic mutation VAF increased following neoadjuvant chemoradiation reflecting decreased ITH (Fig. 5D).

**Discussion**

We developed a murine model to control for irradiation-induced TMB while varying defined states of ITH, thereby enabling investigation of their causal effects on tumor immunogenicity as assessed by response to ICI (Fig. 1). Irradiation induced a sustained increase in TMB and resulting *de novo* neoantigens in tumor forming daughter cells. During tumor evolution, mutations in the founding cell are propagated as clonal/public (VAF > 0.25) whereas mutations arising within a subset are subclonal/private [28]. Irradiated-L tumors showed a sustained decrease in clonal diversity and ITH as evidenced by substantial shifts in tumor somatic mutation VAF and oligoclonal expansion of neoantigens (Fig. 2). Irradiated-L and irradiated-H tumors grew slower than unirradiated parental tumors (Fig. 3), but in the absence of subsequent ICI, implantation of previously irradiated cells alone conferred only a modest survival benefit (Fig. 4, Supplementary Figure 2). Unirradiated parental tumors failed to respond to single or dual  $\alpha$ -PD-L1 and  $\alpha$ -CTLA-4 therapy (Figs. 3 and 4). However, the irradiated-H and irradiated-L models showed significantly improved overall survival with dual ICI; the irradiated-L model showed the most robust improvement with a near doubling of median overall survival (Fig. 4). Only the irradiated-L model showed a benefit from single agent ICI (Fig. 4). Clinically correlated data from patients with rectal adenocarcinoma showed an increase in TMB and decrease in ITH following neoadjuvant radiotherapy consistent with findings in our murine model (Fig. 5).

The identification of ITH as a modulator of response to ICI following irradiation has important translational implications. Multiple studies demonstrate an enhanced response to ICI among patients with prior radiation. However, the etiology of this synergy is debated and primarily centers on mechanisms of *in situ* vaccination via induction of immunogenic tumor death, release of tumor-specific antigens/pro-inflammatory cytokines, and alterations to the tumor microenvironment, among others [2,29–33]. Low ITH and high TMB in the *de novo* treatment setting are potential predictors of response to ICI [13,14]. TMB, irrespective of prior irradiation, has been investigated as a predictor of therapeutic response across various histologies but alone is typically insufficient to predict benefit from ICI [6,13,34–40].

The present study proposes radiation as a modality to augment TMB and clonal neoantigen burden while decreasing ITH to intentionally potentiate ICI response building upon prior studies that show radiation widens the therapeutic window of ICI by increasing expression of immunogenic neoantigens [41,42]. In our murine model irradiation-induced changes in neoantigen expression and alterations in TMB were sustained throughout subsequent tumor formation and growth consistent with prior investigations showing lasting effects of irradiation and cytoreductive treatments on tumor evolution including subclonal expansion and reduced subclonal heterogeneity in glioblastoma multiforme and neuroblastoma [43,44]. Optimization of radiation dose and frac-

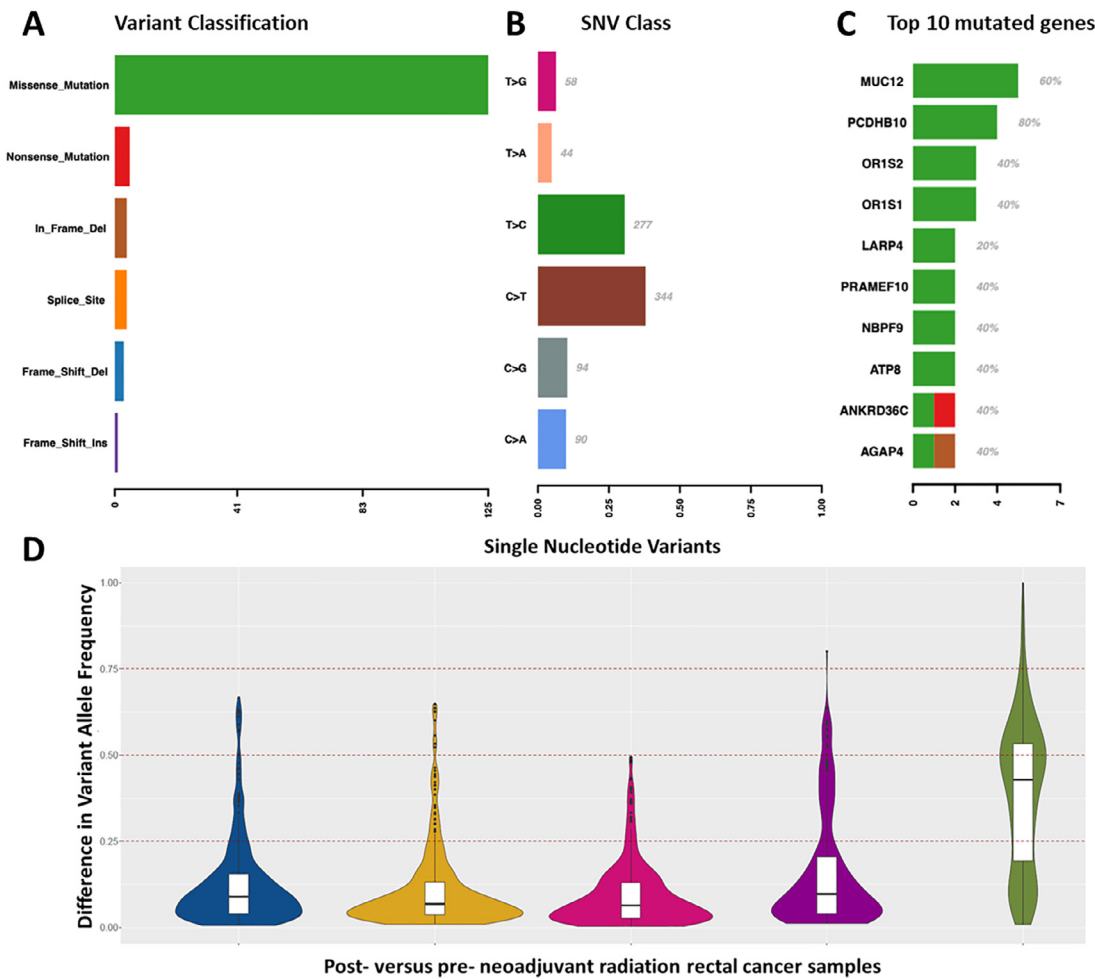


**Fig. 5.** Tumor mutation burden and variant allele frequency shifts between matched pretreatment primary and post-neoadjuvant irradiation rectal adenocarcinoma samples on whole exome sequencing. **A.** Histogram with frequency of identified mutational classes **B.** Histogram with frequency of single nucleotide variants **C.** Ten genes most frequently mutated following irradiation **D.** Violin plot of changes in variant allele frequencies between matched pretreatment primary and post-neoadjuvant irradiation rectal adenocarcinoma samples. Exome sequencing detected increases in single nucleotide variant allele frequency post-irradiation across all 5 paired samples (metric, range): median 0.06-0.43, lower quartile 0.03-0.19, upper quartile 0.13-0.53, minimum 0.004-0.01, maximum 0.27-1.00.

tionation to promote *in situ* vaccination is an active area of research [2,41,45–47]. For example, in preclinical models, the PULSAR approach (ablative radiation doses given in temporally spaced pulses) achieved better tumor control in combination with ICI compared to traditionally fractionated radiation [47]. Our data is compatible with the hypothesis that low ITH versus high ITH facilitates sustained immune recognition of clonal tumor neoantigens [12–14]. Further, irradiation has been shown to induce increased expression of PD-L1 and immunosuppressive checkpoint ligands which may further contribute to the synergy of radiotherapy and ICI observed in our murine model [48,49]. In context with the preceding literature, our study, suggests investigation of combined-modality treatment regimens should consider methods to leverage radiation-induced changes in TMB and ITH to maximize responses to ICI.

Our study has several important strengths and limitations. Irradiation of tumor cells prior to implantation enabled definition of precise states of ITH in our model and control for non-genetic irradiation effects including target volume and dose-dependent alterations to the tumor microenvironment that influence tumor immunogenicity [50]. We performed WES on parental and irradiated tumors grown *in vivo* rather than immediately post-irradiation *in vitro* facilitating analysis of sustained and therefore likely therapeutically relevant alterations in patterns of TMB and ITH. While the present murine model may not directly simulate the *de novo* treatment setting, it bears fidelity to critical clinical

scenarios including use of adjuvant immunotherapy, treatment of local/metastatic post-irradiation recurrences and suggests that previously irradiated relapsed or residual tumors may be more likely to respond to ICI. Our murine model studies were limited to one cell line – the well-characterized B16F10 cell line. Additional validation of pre-clinical studies would demonstrate the reproducibility of our findings. Though the sample size for our clinically correlated data was limited, our data from patients with rectal cancer underscores a similar effect of radiation on TMB and ITH across a spectrum of histologies.

In conclusion, we demonstrate ITH modulates response to ICI following irradiation. Tumors derived from irradiated cells with low ITH responded most robustly to ICI. Our data suggests irradiation is a mechanism via which ITH may be modulated to optimize response to ICI and in concert with prior preclinical and clinical studies further supports therapy paradigms and clinical trials that integrate radiation and immunotherapy.

**Ethics approval and consent to participate**

All appropriate ethics approvals and consents were obtained from the Ethics Committee of Liaoning Cancer Hospital & Institute; University of North Carolina Animal Care and Use Committee.

## Patient consent for publication

Not required.

## Availability of data and material

Research data are stored in an institutional repository and will be shared upon request to the corresponding author.

## Funding

This work as supported by the University Cancer Research Fund from the University of North Carolina. A.Z.W. was also supported by the National Institutes of Health Center for Nanotechnology Excellence Grant U54-CA151652 and R01CA178748.

## Authors' contributions

SS and JW composed the original manuscript. Generating and/or interpreting data were done by JW, SS, YQ, GG, LL, JZ, DM, NK, IK, KW, YZ, TZ, AW. All authors reviewed and proof read the manuscript. Supervision and oversight were done by YZ, GG and AW.

## Authors' information (optional)

Not applicable; please see above for contact information.

## Declaration of Competing Interest

The authors declare no relevant conflict of interest. Full disclosures are provided. TZ has received research funding to institution from Acerta Pharma, Astellas Pharma, Janssen, Merrimack, Merck, Mirati Therapeutics, Novartis, OmniSeq, Personal Genome Diagnostics, Pfizer, Regeneron, StemCentRx; consulting or advisory roles at Amgen, AstraZeneca, Bristol-Myers Squibb, Calithera Biosciences, Dendreon, Exelixis, Foundation Medicine, Genentech/Roche, Janssen, Pharmacyclics, Pfizer, Sanofi, SeaGen, and QED Therapeutics; Honoraria from Exelixis, Genentech/Roche, MJH Life Science, Pacific Genuity; speaker's bureau at Genomic Health and Sanofi/Aventis; stock and other ownership interests at Archimmune Therapeutics (immediate family member), Capio Biosciences (immediate family member), and Nanorobotics (immediate family member). AZW has received research funding from Varian and is a cofounder of Archimmune Therapeutics and Capio Sciences. He also serves on the scientific board of Nanorobotics.

## CRediT authorship contribution statement

**Jie Wang:** Writing – original draft, Writing – review & editing, Investigation, Visualization, Formal analysis, Data curation, Investigation, Methodology. **Shivani Sud:** Writing – original draft, Writing – review & editing, Visualization, Formal analysis, Data curation, Visualization. **Yanli Qu:** Investigation, Writing – review & editing, Resources. **Liantao Li:** Investigation, Writing – review & editing. **Jiajie Zhang:** Investigation, Writing – review & editing. **David Marron:** Investigation, Writing – review & editing. **Nicole Michelle Knape:** Investigation, Writing – review & editing. **Isaiah James Kim:** Investigation, Writing – review & editing. **Kyle Thomas Wagner:** Investigation, Writing – review & editing. **Tian Zhang:** Investigation, Writing – review & editing. **Yuxia Zhao:** Resources, Writing – review & editing, Supervision, Project administration, Resources. **Genyan Guo:** Writing – review & editing, Investigation, Supervision, Project administration, Resources. **Andrew Z. Wang:** Conceptualization, Resources, Writing – review & editing, Supervision, Project administration, Methodology, Funding acquisition.

## Acknowledgements

Not applicable

## Supplementary materials

Supplementary material associated with this article can be found, in the online version, at doi:10.1016/j.neo.2022.100864.

## References

- [1] A Haslam, V. Prasad, Estimation of the Percentage of US Patients With Cancer Who Are Eligible for and Respond to Checkpoint Inhibitor Immunotherapy Drugs, *JAMA Netw Open* 2 (5) (2019) e192535.
- [2] JC Jagodinsky, PM Harari, ZS. Morris, The Promise of Combining Radiation Therapy With Immunotherapy, *International Journal of Radiation Oncology\* Biology\* Physics* 108 (1) (2020) 6–16.
- [3] JE Gray, et al., Three-Year Overall Survival with Durvalumab after Chemoradiotherapy in Stage III NSCLC-Update from PACIFIC, *J Thorac Oncol* 15 (2) (2020) 288–293.
- [4] RH Pierce, JS Campbell, SI Pai, JD Brody, HE. Kohrt, In-situ tumor vaccination: Bringing the fight to the tumor, *Human Vaccines & Immunotherapeutics* 11 (8) (2015) 1901–1909.
- [5] ME Rodriguez-Ruiz, I Vitale, KJ Harrington, I Melero, L. Galluzzi, Immunological impact of cell death signaling driven by radiation on the tumor microenvironment, *Nat Immunol* 21 (2) (2020) 120–134.
- [6] AM Goodman, et al., Tumor Mutational Burden as an Independent Predictor of Response to Immunotherapy in Diverse Cancers, *Mol Cancer Ther* 16 (11) (2017) 2598–2608.
- [7] FA Giordano, MR Veldwijk, C Herskind, F. Wenz, Radiotherapy, tumor mutational burden, and immune checkpoint inhibitors: time to do the math, *Strahlenther Onkol* 194 (10) (2018) 873–875.
- [8] R Mandal, et al., Genetic diversity of tumors with mismatch repair deficiency influences anti-PD-1 immunotherapy response, *Science* 364 (6439) (2019) 485–491.
- [9] SD Brown, et al., Neo-antigens predicted by tumor genome meta-analysis correlate with increased patient survival, *Genome Res* 24 (5) (2014) 743–750.
- [10] DT Le, et al., Mismatch repair deficiency predicts response of solid tumors to PD-1 blockade, *Science* 357 (6349) (2017) 409–413.
- [11] SC Formenti, et al., Radiotherapy induces responses of lung cancer to CTLA-4 blockade, *Nat Med* 24 (12) (2018) 1845–1851.
- [12] M Gerlinger, et al., Intratumor Heterogeneity and Branched Evolution Revealed by Multiregion Sequencing, *N Engl J Med* 366 (10) (2012) 883–892.
- [13] N McGranahan, et al., Clonal neoantigens elicit T cell immunoreactivity and sensitivity to immune checkpoint blockade, *Science* 351 (6280) (2016) 1463–1469.
- [14] Y Wolf, et al., UVB-Induced Tumor Heterogeneity Diminishes Immune Response in Melanoma, *Cell* 179 (1) (2019) 219–235 e21.
- [15] H Li, R. Durbin, Fast and accurate long-read alignment with Burrows-Wheeler transform, *Bioinformatics* 26 (5) (2010) 589–595.
- [16] K Cibulskis, et al., Sensitive detection of somatic point mutations in impure and heterogeneous cancer samples, *Nat Biotechnol* 31 (3) (2013) 213–219.
- [17] J Chen, EE Bardes, BJ Aronow, AG. Jegga, ToppGene Suite for gene list enrichment analysis and candidate gene prioritization, *Nucleic Acids Res* 37 (Web Server issue) (2009) W305–W311.
- [18] W McLaren, et al., The Ensembl Variant Effect Predictor, *Genome Biol* 17 (1) (2016) 122.
- [19] CA Miller, et al., Visualizing tumor evolution with the fishplot package for R, *BMC Genomics* 17 (1) (2016) 880.
- [20] J Hundal, et al., pVAC-Seq: A genome-guided in silico approach to identifying tumor neoantigens, *Genome Med* 8 (1) (2016) 11.
- [21] A Dobin, et al., STAR: ultrafast universal RNA-seq aligner, *Bioinformatics* 29 (1) (2013) 15–21.
- [22] B Li, CN. Dewey, RSEM: accurate transcript quantification from RNA-Seq data with or without a reference genome, *BMC Bioinformatics* 12 (1) (2011) 323.
- [23] Picard Toolkit [Internet]. *Broad Institute, GitHub repository* [published online ahead of print: 2020]; <http://broadinstitute.github.io/picard/>. cited
- [24] Poplin R et al. *Scaling accurate genetic variant discovery to tens of thousands of samples* [Internet]. *Genomics*; 2017:
- [25] Van der Auwera GA, O'Connor BD. *Genomics in the cloud: using Docker, GATK, and WDL in Terra* [Internet]. 2020:
- [26] K Wang, M Li, H. Hakonarson, ANNOVAR: functional annotation of genetic variants from high-throughput sequencing data, *Nucleic Acids Research* 38 (16) (2010) e164.
- [27] V Boeva, et al., Control-FREEC: a tool for assessing copy number and allelic content using next-generation sequencing data, *Bioinformatics* 28 (3) (2012) 423–425.
- [28] MJ Williams, B Werner, CP Barnes, TA Graham, A. Sottoriva, Identification of neutral tumor evolution across cancer types, *Nat Genet* 48 (3) (2016) 238–244.
- [29] F Manapov, O Roengvoraphoj, C. Eze, Why is survival after pembrolizumab affected by previous radiotherapy? *The Lancet Oncology* 18 (9) (2017) e504.
- [30] SC Formenti, S. Demaria, Radiation therapy to convert the tumor into an in situ vaccine, *Int J Radiat Oncol Biol Phys* 84 (4) (2012) 879–880.
- [31] AB Sharabi, M Lim, TL DeWeese, CG. Drake, Radiation and checkpoint blockade immunotherapy: radiosensitisation and potential mechanisms of synergy, *Lancet Oncol* 16 (13) (2015) e498–e509.
- [32] WSM Theelen, et al., Pembrolizumab with or without radiotherapy for metastatic non-small-cell lung cancer: a pooled analysis of two randomised trials, *Lancet Respir Med* 9 (5) (2021) 467–475.
- [33] N Shaverdian, et al., Previous radiotherapy and the clinical activity and toxicity of pembrolizumab in the treatment of non-small-cell lung cancer: a secondary analysis of the KEYNOTE-001 phase 1 trial, *The Lancet Oncology* 18 (7) (2017) 895–903.

- [34] N Andor, et al., Pan-cancer analysis of the extent and consequences of intratumor heterogeneity, *Nat Med* 22 (1) (2016) 105–113.
- [35] DT Le, et al., PD-1 Blockade in Tumors with Mismatch-Repair Deficiency, *N Engl J Med* 372 (26) (2015) 2509–2520.
- [36] MD Hellmann, et al., Nivolumab plus Ipilimumab in Lung Cancer with a High Tumor Mutational Burden, *N Engl J Med* 378 (22) (2018) 2093–2104.
- [37] NA Rizvi, et al., Cancer immunology. Mutational landscape determines sensitivity to PD-1 blockade in non-small cell lung cancer, *Science* 348 (6230) (2015) 124–128.
- [38] A Snyder, et al., Genetic Basis for Clinical Response to CTLA-4 Blockade in Melanoma, *N Engl J Med* 371 (23) (2014) 2189–2199.
- [39] EM Van Allen, et al., Genomic correlates of response to CTLA-4 blockade in metastatic melanoma, *Science* 350 (6257) (2015) 207–211.
- [40] D Liu, et al., Integrative molecular and clinical modeling of clinical outcomes to PD1 blockade in patients with metastatic melanoma, *Nat Med* 25 (12) (2019) 1916–1927.
- [41] DM Lussier, et al., Radiation-induced neoantigens broaden the immunotherapeutic window of cancers with low mutational loads, *Proc Natl Acad Sci USA* 118 (24) (2021) e2102611118.
- [42] C Lhuillier, et al., Radiotherapy-exposed CD8+ and CD4+ neoantigens enhance tumor control, *J Clin Invest* 131 (5) (2021) 138740.
- [43] JH McAbee, et al., Radiation Drives the Evolution of Orthotopic Xenografts Initiated from Glioblastoma Stem-like Cells, *Cancer Res* 79 (23) (2019) 6032–6043.
- [44] A Schramm, et al., Mutational dynamics between primary and relapse neuroblastomas, *Nat Genet* 47 (8) (2015) 872–877.
- [45] HB Barsoumian, et al., Low-dose radiation treatment enhances systemic antitumor immune responses by overcoming the inhibitory stroma, *J Immunother Cancer* 8 (2) (2020) e000537.
- [46] MZ Dewan, et al., Fractionated but Not Single-Dose Radiotherapy Induces an Immune-Mediated Abscopal Effect when Combined with Anti-CTLA-4 Antibody, *Clin Cancer Res* 15 (17) (2009) 5379–5388.
- [47] C Moore, et al., Personalized Ultrafractionated Stereotactic Adaptive Radiotherapy (PULSAR) in Preclinical Models Enhances Single-Agent Immune Checkpoint Blockade, *Int J Radiat Oncol Biol Phys* 110 (5) (2021) 1306–1316.
- [48] A Derer, et al., Chemoradiation Increases PD-L1 Expression in Certain Melanoma and Glioblastoma Cells [Internet], *Front. Immunol.* 7 (2016), doi:10.3389/fimmu.2016.00610.
- [49] J Gong, TQ Le, E Massarelli, AE Hendifar, R. Tuli, Radiation therapy and PD-1/PD-L1 blockade: the clinical development of an evolving anticancer combination, *J. immunotherapy cancer* 6 (1) (2018) 46.
- [50] HE Barker, JTE Paget, AA Khan, KJ. Harrington, The tumour microenvironment after radiotherapy: mechanisms of resistance and recurrence, *Nat Rev Cancer* 15 (7) (2015) 409–425.